

# Photon Berry phases, Instantons and Schrodinger Cats with oscillating parities in cavity QED

Yu Yi-Xiang<sup>1,2</sup>, Jinwu Ye<sup>1,3</sup>, W.M. Liu<sup>2</sup> and CunLin Zhang<sup>3</sup>

<sup>1</sup> *Department of Physics and Astronomy, Mississippi State University, P. O. Box 5167, Mississippi State, MS, 39762*

<sup>2</sup> *Beijing National Laboratory for Condensed Matter Physics,  
Institute of Physics, Chinese Academy of Sciences, Beijing 100190, China*

<sup>3</sup> *Key Laboratory of Terahertz Optoelectronics, Ministry of Education,  
Department of Physics, Capital Normal University, Beijing 100048, China*

(Dated: March 8, 2019)

The four standard quantum optics model in cavity QED such as Rabi, Dicke, Jaynes-Cummings ( JC ) and Tavis-Cummings (TC) model were proposed many decades ago. Despite their relative simple forms and many previous theoretical works, their solutions at a finite  $N$  inside the superradiant regime remain unknown. In view of recent remarkable experimental advances in several experimental systems such as cold atoms inside a cavity or superconducting qubits inside a microcavity to realize these models, it becomes topical and important to understand what would be the new phenomena in these models at a finite  $N$ , especially inside the superradiant regime. In this work, we resolved this outstanding problem. We use three independent methods such as  $1/J$  expansion, the strong coupling expansion and exact diagonalization (ED) to study  $U(1)/Z_2$  Dicke model at a finite  $N$  and different anisotropy parameters  $0 \leq \beta \leq 1$  as the atom-photon interaction strength increases. This model include the four standard quantum optics model as its special limit. We identify 4 different regimes: the normal,  $U(1)$ , strong quantum tunneling (QT) and weak QT regime. In the strong QT regime, by the non-perturbative instanton method, we find the emergencies of bound states one by one as the interaction strength increases, then investigate a new class of quantum tunneling processes through the instantons between the two bound states in the compact photon phase leading to Schrodinger Cats oscillating with even and odd parities. We find it is the Berry phase interference effects in the instanton tunneling event which leads to the oscillations. In the weak QT regime, we employ a strong coupling expansion and find results smoothly connected with those in the strong QT regime, especially recover the dramatic Berry phase interference effects from a completely different approach. In the  $Z_2$  limit, all the zeros due to the Berry phase are pushed to infinity, the so the ground state always has even parity with no oscillations. We map out the evolution of energy level structures and also compute the photon correlation functions, squeezing spectrum and number correlation functions. We find nearly perfect agreements between the strong coupling expansion and the ED not only in the weak and strong QT regimes, but also in the  $U(1)$  regime not too close to the critical point at  $N = \infty$ . The combination of the three methods lead to rather complete physical pictures in the whole crossover regimes from the  $U(1)$  Dicke to the  $Z_2$  Dicke model. Experimental realizations and detections are presented. Connections with past works and future perspectives are also discussed.

## 1. Introduction–

Quantum optics is a subject to describe the atom-photon interactions [1–3]. The history of quantum optics can be best followed by looking at the evolution of quantum optics models to study such interactions. In the Rabi model proposed in 1937 [4], a single mode photon interacts with a two level atom with equal rotating wave (RW) and counter rotating wave (CRW) strength. To study possible many body effects such as "optical bombs", a single two level atoms in the Rabi model was extended to an assembly of  $N$  two level atoms in the Dicke model [5] advanced in 1954. When the coupling strength is well below the transition frequency, the CRW term in the Rabi model is effectively much smaller than that of RW, so it was dropped in the Jaynes-Cummings ( JC ) model [6] put forward in 1963. Similar to the generalization from the Rabi to the Dicke model, the single two level atom in the JC model was extended to an assembly of  $N$  two level atoms in the Tavis-Cummings (TC) model [7] advocated in 1968. The TC model was studied in the

thermodynamic limit  $N \rightarrow \infty$  in [8–11] A superradiant phase transition was found and a zero mode identified in the superradiant phase. The Dicke model in the thermodynamic limit  $N \rightarrow \infty$  was studied in [12] and level statistics was found to change from Poissonian distribution to Wigner-Dyson one from normal to the superradiant phase.

It is convenient to classify the four well known quantum optics models from a simple symmetry point of view: the TC and Dicke model as  $U(1)$  and  $Z_2$  Dicke model respectively, while JC and Rabi model are just as the  $N = 1$  version of the two [15, 16]. In fact, as stressed in [16], there are also two different representations on all of the 4 models:  $N$ – representation with  $N$  independent two level atoms with a large Hilbert space  $2^N$  and spin  $J = N/2$  representation with a smaller Hilbert space  $N + 1$ . The dramatic finite size effects such as the Berry phase effects, Goldstone and Higgs modes on  $U(1)$  Dicke model were thoroughly discussed in both  $N$ – representation in [15] by  $1/N$  expansion and spin- $J = N/2$

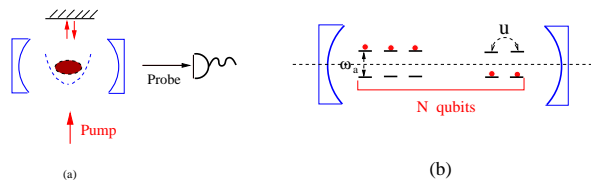


FIG. 1. (a) Cold or thermal atoms in a trap embedded in a cavity in the strong coupling regime with a transverse pumping [27–29]. The probe detects the Fluorescence spectrum of the cavity leaking photons. (b)  $N = 2 \sim 9$  superconducting qubits are placed on the one or more anti-nodes of a circuit QED resonator [22–26].

representation [16] by  $1/J$  representation. Remarkably, we find nearly perfect agreements between the results achieved by  $1/N$  and  $1/J$  and the ED studies even when  $N$  gets to its lowest value  $N = 1$ . The relations between the two representations were also clarified in [16]. The effects of a small CRW term near the  $U(1)$  Dicke model was also studied in [16]. There are also formally exact Bethe Ansatz-like solution for the integrable  $U(1)$  Dicke model at a finite  $N$  [17]. Recently, a formal exact solution was found even for the non-integrable  $Z_2$  Dicke model at  $N = 1$  ( Rabi model ) [18]. Unfortunately, it is not known how to extract any important physics from these formally exact solutions even at  $N = 1$ . For the Dicke model, the ground state photon number at the QCP ( Fig.2 ) was found to scale as  $N^{1/3}$  [13] which is a direct consequence of finite size scaling near a QCP with infinite coordination numbers [14]. In view of the tremendous success of the  $1/N$  and  $1/J$  expansion in studying many strongly correlated electron systems [19, 35], particularly in the  $U(1)$  Dicke model achieved in [15, 16], it is natural to apply them to study the  $Z_2$  Dicke model as originally planned in [15].

Due to recent tremendous advances in technologies, the TC model was successfully achieved in at least two experimental systems (1) with a BEC of  $N \sim 10^5$   $^{87}\text{Rb}$  atoms inside an ultrahigh-finesse optical cavity [20, 21] and (2) superconducting qubits inside a microwave circuit cavity [22–24, 26] or quantum dots inside a semiconductor microcavity [25]. The superradiant phase in the Dicke model was also realized in system (1) with the help of transverse pumping ( Fig.1a ) [27–29]. It could also be realized “spontaneously” in the system (2) without external pumping [16]. Indeed, by enhancing the inductive coupling of a flux qubit to a transmission line resonator, a remarkable ultra-strong coupling with individual  $\tilde{g} \sim 0.12\omega_a$  was realized in a circuit QED system [26]. However, in such a ultra-strong coupling regime, the system is described well neither by the TC model nor the Dicke model, but a combination of the two Eqn.1 with unequal RW and CRW strength dubbed as  $U(1)/Z_2$  Dicke model in [16]. It was also proposed in [30] that in the thermal or cold atom experiments, the strengths of

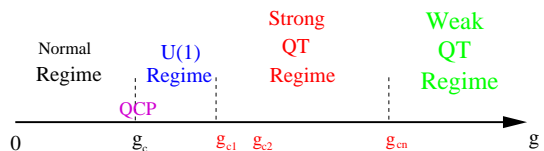


FIG. 2. The four regimes in the  $U(1)/Z_2$  Dicke model at a finite  $N$  as the coupling  $g$  increases at a fixed anisotropy parameter  $0 < g'/g = \beta < 1$ . The quantum critical point ( QCP ) at  $N = \infty$  is at  $g_c = \sqrt{\omega_a\omega_b}/(1 + \beta)$ . All regimes can be realized in various current experimental systems in Fig.1. This paper focus on the three regimes away from the QCP [34]. The  $U(1)$  regime may disappear if  $\beta$  [16] gets too close to 1.

$g$  and  $g'$  can be tuned separately by using circularly polarized pump beams in a ring cavity. Indeed, based on the scheme, a recent experiment [31] attempted to realize the  $U(1)/Z_2$  Dicke model with continuously tunable  $g$  and  $g'$ . As argued in [15, 16], with only a few  $N = 2 \sim 12$  qubits embedded in system (2), the finite size effects may become important and experimentally observable. With the recent advances of manipulating a few to a few hundreds of cold atoms inside an optical cavity in system (1) [32, 33], the finite size effects may also become important and experimentally observable in near future experiments on system (1). As advocated in [16], in any case, the Hamiltonian Eqn.1 with independent  $g$  and  $g'$  is the most general Hamiltonian describing various experimental systems in various coupling regimes under the two atomic levels and a single photon mode approximation. In [16], we focused on the  $U(1)/Z_2$  Dicke model Eqn.1 near the  $U(1)$  limit ( namely, with a small anisotropy parameter  $g'/g = \beta \ll 1$  and not too far from the critical strength  $g_c$  ) at any finite  $N$ . Here, we will study many novel quantum phenomena in the  $U(1)/Z_2$  Dicke model Eqn.1 at any  $\beta$ , interaction strength and  $N$ .

The  $U(1)/Z_2$  Dicke model is described by:

$$H_{U(1)/Z_2} = \omega_a a^\dagger a + \omega_b J_z + \frac{g}{\sqrt{2J}}(a^\dagger J_- + a J_+) + \frac{g'}{\sqrt{2J}}(a^\dagger J_+ + a J_-) \quad (1)$$

where the  $\omega_a, \omega_b$  are the cavity photon frequency and the energy difference of the two atomic levels respectively, the  $g = \sqrt{N}\tilde{g}$  is the collective photon-atom coupling (  $\tilde{g}$  is the individual photon-atom coupling ). The  $g' = \sqrt{N}\tilde{g}'$  is the counter-rotating wave term. We fix their ratio  $0 < g'/g = \beta < 1$ . If  $\beta = 0$ , the Hamiltonian Eqn.1 has the  $U(1)$  symmetry  $a \rightarrow ae^{i\theta}, \sigma^- \rightarrow \sigma^- e^{i\theta}$  with a conserved quantity  $P = a^\dagger a + J_z$ . The CRW  $g'$  term breaks the  $U(1)$  to the  $Z_2$  symmetry  $a \rightarrow -a, \sigma^- \rightarrow -\sigma^-$  with the parity operator  $\Pi = e^{i\pi(a^\dagger a + J_z)}$ . If  $\beta = 1$ , it becomes the  $Z_2$  Dicke model.

In this paper, we study novel quantum phenomena in the  $U(1)/Z_2$  Dicke model Eqn.1 in its spin  $J = N/2$  rep-

resentation at a finite  $N$ , any interaction strength  $g$  and anisotropy parameter  $0 < \beta < 1$  by 3 independent methods:  $1/J$  expansion [16], strong coupling expansion [35] and ED [12, 16]. As a fixed  $\beta$ , as the  $g$  increases, we identify 4 different crossover regimes: the normal,  $U(1)$ , the strong quantum tunneling (QT) regime and weak QT regime Fig.2. In the strong QT regime, by the WKB approximation, we find the emergencies of bound states one by one as the  $g$  increases. We then investigate a new class of quantum tunneling processes due to instantons between the two bound states in the compact photon phase. It leads to Schrodinger Cats with oscillating even and odd parities in both ground and higher energy bound states. It is the Berry phase interference effects in the instanton tunneling event which causes the oscillations. In the weak QT regime, we employ a strong coupling expansion to study the even-odd parity state splittings in both the ground state and the low energy excited states. We find that it is the anisotropy parameters  $\beta < 1$  which leads to the gap closing and the alternating even-odd parity in the ground state and low energy excited state. We also compute the photon correlation functions, squeezing spectrum and number correlation functions which can be detected by Fluorescence spectrum, phase sensitive homodyne detection and Hanbury-Brown-Twiss (HBT) type of experiments respectively [36]. We map out the evolution of the energy levels from the  $U(1)$  regime to the strong and weak QT regimes in Fig.5. We find nearly perfect agreements between the strong coupling expansion and the ED not only in the QT regimes, but also in the  $U(1)$  regime not too close to the critical point at  $N = \infty$ . The physics at the  $Z_2$  limit could be well understood by taking  $\beta \rightarrow 1^-$  limit. The combination of the Instanton method, strong coupling expansion and the ED lead to rather complete physical pictures in the whole crossover regimes from the  $U(1)$  Dicke to the  $Z_2$  Dicke model in Fig.2. Experimental realizations, especially the preparations and detections of the Schrodinger Cats in both experimental systems are discussed. Connections with the previous works are speculated and future perspectives are outlined.

## 2. $1/J$ expansion in the super-radiant phase

Following [16], inside the super-radiant phase [34], it is convenient to write both the photon and atom in the polar coordinates  $a = \sqrt{\lambda_a^2 + \delta\rho_a} e^{i\theta_a}$ ,  $b = \sqrt{\lambda_b^2 + \delta\rho_b} e^{i\theta_b}$ . When performing the controlled  $1/J$  expansion, we keep the terms to the order of  $\sim j$ ,  $\sim 1$  and  $\sim 1/j$ , but drop orders of  $1/j^2$  or higher. We first minimize the ground state energy at the order  $j$  and found the saddle point values of  $\lambda_a$  and  $\lambda_b$ :

$$\lambda_a = \frac{g+g'}{\omega_a} \sqrt{\frac{j}{2}(1-\mu^2)}, \quad \lambda_b = \sqrt{j(1-\mu)} \quad (2)$$

where  $\mu = \omega_a\omega_b/(g+g')^2$ . In the superradiant phase  $g+g' > g_c = \sqrt{\omega_a\omega_b}$ . In the normal phase  $g+g' < g_c$ , one gets back to the trivial solution  $\lambda_a = \lambda_b = 0$ .

Observe that (1) in the superradiant phase  $g(1+\alpha) > g_c$ ,  $\lambda_a^2 \sim \lambda_b^2 \sim j$ , (2) it is convenient to introduce the  $\pm$  modes:  $\theta_{\pm} = (\theta_a \pm \theta_b)/2$ ,  $\delta\rho_{\pm} = \delta\rho_a \pm \delta\rho_b$ ,  $\lambda_{\pm}^2 = \lambda_a^2 \pm \lambda_b^2$ . (3) Defining the Berry phase in the + sector [15] as  $\lambda_+^2 = P + \alpha$  where  $P = 1, 2, \dots$  is the closest integer to the  $\lambda_+^2$ , so  $-1/2 < \alpha < 1/2$ . We can neglect the Berry phase in the - sector. (4) after shifting  $\theta_{\pm} \rightarrow \theta_{\pm} + \pi/2$ , we reach the Hamiltonian to the order of  $1/j$ :

$$\mathcal{H}[\delta\rho_{\pm}, \theta_{\pm}] = \frac{D}{2}(\delta\rho_+ - \alpha)^2 + D_-[\delta\rho_- + \gamma(\delta\rho_+ - \alpha)]^2 + 4\omega_a\lambda_a^2\left[\frac{1}{1+\beta}\sin^2\theta_- + \frac{\beta}{1+\beta}\sin^2\theta_+\right] \quad (3)$$

where  $D = \frac{2\omega_a(g+g')^2}{E_H^2 N}$  is the phase diffusion constant in the + sector,  $D_- = E_H^2/16\lambda_a^2\omega_a$  with  $E_H^2 = (\omega_a + \omega_b)^2 + 4(g+g')^2\lambda_a^2/N$ . The  $\gamma = \frac{\omega_a^2}{E_H^2}(1 - \frac{(g+g')^4}{\omega_a^4})$  is the coupling between the + and - sector.

Note that for  $\beta < 1$ , the condition to reach the superradiant regime  $4\lambda_a^2\frac{\beta}{1+\beta} \gg 1$  is more stringent than the large  $J$  expansion condition  $\lambda_a^2 \gg 1$ . In the  $j \rightarrow \infty$  limit, it holds for any  $g > g_c$ , but leads to a constraint on  $g$  at a finite  $j$ . In this regime, one can simply set  $\sin^2\theta_{\pm} \sim \theta_{\pm}^2$  in Eqn.3 which becomes a quadratic theory. It can be easily diagonalized and lead to one low energy gapped pseudo-Goldstone mode and a high energy gapped optical mode. Setting  $\beta = 1$  recovers the results for the  $Z_2$  Dicke model in the superradiant phase at  $N = \infty$  in [12].

If one neglects the quantum fluctuations of the  $\theta_-$  mode, namely, by setting  $\theta_-$  at its classical value  $\theta_- = 0$ , Eqn.3 is simplified to:

$$\mathcal{H}_+[\delta\rho_+, \theta_+] = \frac{D}{2}(\delta\rho_+ - \alpha)^2 + 2\omega_a\lambda_a^2\frac{2\beta}{1+\beta}\sin^2\theta_+ \quad (4)$$

where  $[\theta_+, \delta\rho_+] = i\hbar$ . This approximation may not give very precise numbers to physical quantities, but do lead to correct qualitative physical picture, especially the topological effects due to the Berry phase in all the physical quantities.

In the superradiant limit  $4\lambda_a^2\frac{\beta}{1+\beta} \gg 1$ , one can identify the approximate atomic mode:

$$\omega_{-0}^2 = 4\omega_a\lambda_a^2\frac{2\beta}{1+\beta}D = \frac{4}{E_H^2}\frac{\beta}{1+\beta}[(g+g')^4 - g_c^4] \quad (5)$$

which is nothing but the pseudo-Goldstone mode due to the CRW  $g'$  term. By neglecting the quantum fluctuations of  $\theta_-$ , the high energy optical mode in the  $\theta_-$  sector does not exist anymore in Eqn.4.

3.  $U(1)$  regime and the formation of consecutive bound states in strong quantum tunneling regime– As shown for the  $U(1)$  Dicke model [15, 16], the following very interesting phenomena happen in the  $\theta_+$  sector : there are consecutive level crossings at  $g_c < g_{c1} < g_{c2} \dots$  in both the ground state and excited states, there are also the corresponding Berry phases in the quantum phase diffusion

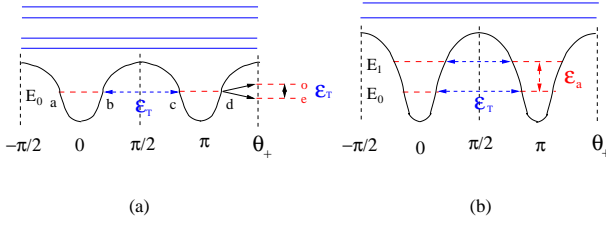


FIG. 3. The bound states and the quantum tunneling processes in the strong tunneling regime in Fig.2. The atomic energy  $\epsilon_a$  and the tunneling energy  $\Delta$  are shown in this figure. But the higher optical energy  $\epsilon_o$  is not shown. (a) At  $g = g_{c1} > g_c = \sqrt{\omega_a\omega_b}/(1 + \beta)$ , the double well potential in the  $\theta_+$  sector in Eqn.4 holds just one bound state with energy  $E_0$  denoted by a red dashed line. The blue dashed line shows the quantum tunneling between the two bound states which leads to a splitting  $\Delta_0$  listed in Eqn.15. The blue solid lines denote scattering states shown in Fig.5b (b) As the  $g$  increases further to  $g = g_{c2} > g_{c1}$ , the lowest two scattering states in (a) also become the second bound state with energy  $E_1 = E_0 + \epsilon_a$ , the third bound state shows up at  $g = g_{c3} > g_{c2} > g_{c1}$  and so on. The excitation energy is the "atomic" energy  $\epsilon_a$ . As explained below Eqn.14, the ground state could also be odd parity depending on  $(-1)^P$ .

mode  $E_D$ , so the  $U(1)$  superradiant phase at a finite  $N$  is signatred by the first crossing after which there are photons and inverted atoms in the ground states with alternating parities. Here for the  $U(1)/Z_2$  Dicke model, very different phenomena happen in the  $\theta_+$  sector given by Eqn.4: as the potential gets deeper and deeper, there are consecutive bound states formations at  $g_c < g_{c1} < g_{c2} \dots$  leading to the "atomic" energy scale  $\omega_a$ . The QT regime is signatred by the first appearance of the bound state after which there are consecutive appearances of more bound states at higher energies ( Fig.3a,b ). The regime  $g_c < g < g_{c1}$  is called  $U(1)$  regime.

One can calculate all these  $g_c < g_{c1} < g_{c2} \dots$  by using the Bohr-Sommerfeld quantization condition  $\int_a^b p d\theta = (n + 1/2)\pi\hbar$ ,  $n = 0, 1, 2, \dots$  where  $p = \sqrt{2m(E_n - V(\theta))}$  and the  $E_n = E_0, E_1, \dots$  is the  $n$ -th bound state energy in Fig.3a,b. From Eqn.4, we can see the  $m = \frac{1}{D}$ ,  $V(\theta) = \omega_a\lambda_a^2 \frac{2\beta}{1+\beta}(1 - \cos 2\theta_+)$  and the  $a$  and  $b$  are the two end points shown in Fig.3a. We find that the bound states emerge at

$$\frac{\omega_{-0}}{D} = (n + 1/2)\frac{\pi}{2}\hbar, \quad n = 0, 1, 2, \dots \quad (6)$$

Note that because the bound state is either localized around  $\theta_+ = 0$  or  $\theta_+ = \pi$ , so the Berry phase  $\alpha$  in Eqn.4 plays no roles, so can be dropped. However, as to be shown in the following section, it does play very important roles in the quantum tunneling process between the two bound states.

When  $\frac{\omega_{-0}}{D} < \frac{\pi}{4}\hbar$ , there is no bound state. Substituting the expression for the diffusion constant  $D$  and the

atomic mode  $\omega_{-0}$  in Eqn.5 leads to:

$$4\lambda_a^2 \sqrt{\frac{\beta}{1 + \beta}} < \frac{\pi}{4} \quad (7)$$

Note that for large  $J$  expansion to apply, one need to require  $\lambda_a^2 > 1$ , So for sufficiently small  $g'/g = \beta$ , there is an appreciable  $U(1)$  regime  $g_c < g < g_{c1}$  before the quantum tunneling regime in Fig.2.

In this  $U(1)$  regime, the second term in Eqn.4 breaks the  $U(1)$  symmetry to  $Z_2$  symmetry, the Goldstone mode at  $N = \infty$  simply becomes a pseudo-Goldstone mode. But its effects at a finite  $N$  is much more delicate to analyze. One can treat the second term in Eqn.4 perturbatively either by non-degenerate or degenerate perturbation expansion. The total excitation  $P$  is not conserved anymore and is replaced by the parity  $\Pi = (-1)^P$ , the energy levels are only grouped into even and odd parities in Fig.5,6. As shown in [16], at a given  $P$  sector,  $m = 0, \pm 1, \dots, \pm P$ , a second order perturbation at  $m = \pm 1$  leads to the maximum gap at  $\alpha = 0$  in Fig.5b:

$$\Delta_{m=\pm 1, U(1)} = \frac{D}{2} - \frac{\omega_a\lambda_a^2}{2} \frac{2\beta}{1 + \beta} \quad (8)$$

Using Eqn.5, one can rewrite  $\Delta = \frac{D}{2}[1 - \frac{1}{2}(\frac{\omega_{-0}}{D})^2] > 0$ . For general  $\pm m$ , one needs  $m$ -th order degenerate perturbation calculation leading to find the the maximum gap  $\Delta_{m, U(1)}$  at  $\alpha = 0$  between the  $m$  and  $m + 1$  crossing in Fig.5b:

$$\Delta_{m, U(1)} = \frac{D}{2}(2m + 1) - R_{m+1} - R_m \quad (9)$$

where  $R_m \sim (\frac{\omega_a\lambda_a^2}{2} \frac{2\beta}{1+\beta})^m$ ,  $m = 0, 1, \dots, P$ ;  $R_0 = 0$  is the gap opening at the  $m + 1$  crossing in the  $U(1)$  limit Eqn.5a. Setting  $m = 0$  recovers Eqn.8.

Nonetheless, the important phenomena of Goldstone and Higgs mode at the  $U(1)$  limit can still be observed in this  $U(1)$  regime after considering this perturbation. Various photon correlation functions in this  $U(1)$  regime will be discussed elsewhere [38].

Now we follow the formation of the bound states just after the  $U(1)$  regime. When  $\frac{\omega_{-0}}{D} = \frac{\pi}{4}\hbar$ , namely  $g = g_{c1}$ , it just holds the first bound state with  $\theta_b = -\theta_a = \frac{\pi}{2}$ ,  $E_1 = 2\omega_a\lambda_a^2 \frac{2\beta}{1+\beta}$ . When  $\frac{\pi}{4}\hbar < \frac{\omega_{-0}}{D} < \frac{3\pi}{4}\hbar$ , it holds the first bound state ( Fig.3a ) with energy  $E_1 = 2\omega_a\lambda_a^2 \frac{2\beta}{1+\beta} \sin^2 \theta_a$  where  $\frac{\omega_{-0}}{D} F(\theta_a) = \frac{\pi}{4}\hbar$ ,  $F(\theta_a) = \int_0^{\theta_a} d\theta \sqrt{\sin^2 \theta_a - \sin^2 \theta}$ ,  $0 < \theta_a < \pi/2$ . It is easy to see  $0 < F(\theta_a) < 1$ ,  $F(\theta_a = \pi/2) = 1$ . When  $\frac{\omega_{-0}}{D} = \frac{3\pi}{4}\hbar$ , namely  $g = g_{c2}$ , it just holds the second bound state with  $\theta_b = -\theta_a = \frac{\pi}{2}$ ,  $E_2 = 2\omega_a\lambda_a^2 \frac{2\beta}{1+\beta}$ . While the first bound state energy is given by  $F(\theta_a) = 1/3$ ,  $E_1 = 2\omega_a\lambda_a^2 \frac{2\beta}{1+\beta} \sin^2 \theta_a$ .

When  $\frac{3\pi}{4}\hbar < \frac{\omega_{-0}}{D} < \frac{5\pi}{4}\hbar$ , it holds two bound states (

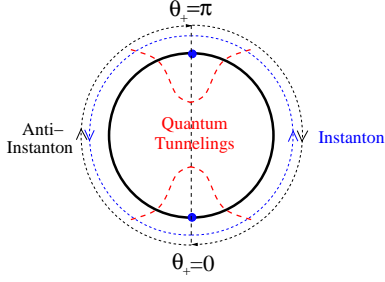


FIG. 4. The quantum tunneling process due to the instantons between the two bound states at  $\theta_+ = 0$  and  $\theta_+ = \pi$ . The counterclockwise (blue dashed line) tunneling is an instanton. The clockwise (black dashed line) tunneling is an anti-instanton.

Fig.3b) with energies:

$$E_1 = 2\omega_a \lambda_a^2 \frac{2\beta}{1+\beta} \sin^2 \theta_{1a}, \quad \frac{\omega_{-0}}{D} F(\theta_{1a}) = \frac{\pi}{4} \hbar$$

$$E_2 = 2\omega_a \lambda_a^2 \frac{2\beta}{1+\beta} \sin^2 \theta_{2a}, \quad \frac{\omega_{-0}}{D} F(\theta_{2a}) = \frac{3\pi}{4} \hbar, \quad (10)$$

where one can identify the first atomic energy in Fig.3a:

$$\epsilon_a = E_2 - E_1 = 2\omega_a \lambda_a^2 \frac{2\beta}{1+\beta} (\sin^2 \theta_{2a} - \sin^2 \theta_{1a}) \quad (11)$$

As expected  $\epsilon_a$  is different than the  $\omega_{-0}$  in Eqn.5.

As  $g \rightarrow \infty$ ,  $D \rightarrow 0$ , while  $\omega_{-0} \rightarrow \sqrt{2}\omega_a \sqrt{\frac{2\beta}{1+\beta}}$ , so the left hand side of Eqn.6 diverges, there are infinite number of bound states. This approaches the weak quantum tunneling regime to be discussed by strong coupling method [35] in the following sections.

#### 4. Quantum tunneling between the two bound states: Berry phase and instantons

The instanton solution for a Sine-Gordon model was well known [39]. From Eqn.4, we can find the classical instanton solution connecting the two minima from  $\theta_+ = 0$  or  $\theta_+ = \pi$ :  $\theta_+(\tau) = 2 \tan^{-1} e^{\omega_{-0}(\tau - \tau_0)}$  where  $\tau_0$  is the center of the instanton. Its asymptotic form as  $\tau \rightarrow \infty$  is  $\theta_+(\tau \rightarrow \infty) \rightarrow \pi - 2e^{-\omega_{-0}(\tau - \tau_0)}$ . The corresponding classical instanton action is:

$$S_0 = \frac{2\omega_{-0}}{D} \quad (12)$$

The instanton problems in three well known systems (1) a double well potential (DWP) in a  $\phi^4$  theory (2) periodic potential problem (PPP) (3) a particle on a circle (POC) are well studied in Refs.[39]. As shown in the following, the tunneling problem in the present problem is related, but different than all the three systems in the following important ways: (1) the potential  $V(\theta) = 2\omega_a \lambda_a^2 \frac{2\beta}{1+\beta} (1 - \cos 2\theta_+)$  in Eqn.4 is a periodic potential in  $\theta_+$ . In this regard, it is different than the  $\phi^4$  theory, but similar to PPP. (2) The  $\theta_+$  is a compact angle confined in  $0 < \theta_+ < 2\pi$ . In this regard, it is

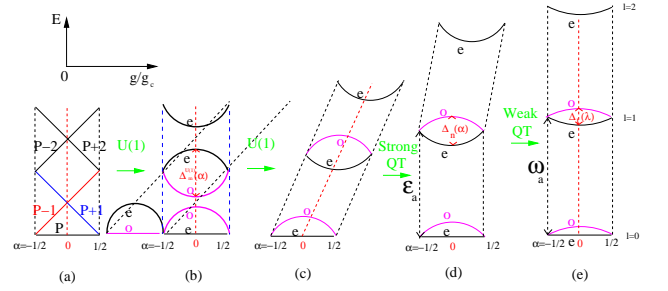


FIG. 5. The (low energy) atomic energy levels from the  $U(1)$  regime to the strong QT regime as  $g$  changes at a fixed  $\beta$ . The ground state energy has been subtracted. In the  $U(1)$  regime, there are  $P$  doublets in (a) and (b) along the vertical (blue) lines. (a) The energy spectrum at the  $U(1)$  limit  $\beta = 0$  [16]. (b) The energy level repulsions between the same parity and crossings between the opposite parity in the  $U(1)$  regime. All the states are scattering states. In the  $U(1)$  regime, if the total excitation  $P$  is even, along the vertical (blue) lines, the doublets are organized as  $(e, o), (o, e), (e, o), (o, e), \dots$ . If  $P$  is odd, one need to flip all the parities. See Fig.7 at  $N = 2, \beta = 0.1$ . (c) In the  $U(1)$  regime, all the states are still scattering states. Here if we follow the ground state with  $P, P+1, P+2, \dots$  at  $l = 0, 1, 2, \dots$  respectively, there are relatively large shifts of zeros to the right. Only the splittings at  $m = \pm 1, \pm 2$  are shown here. See Fig.8 at  $N = 2, \beta = 0.5$ . The doublet at  $l = 0$  could also be the first bound state at  $l = 0$ , then the states at  $l = 1, \dots$  remain scattering states as shown in Fig.3a. (d) In the QT regime, the two states at  $l = 0, 1$  are bound states which are connected by nearly straight boundaries at  $\alpha = -1/2, 0, 1/2$ . The states at  $l = 2, \dots$  remain scattering states as shown in Fig.3b. See Fig.9 at  $N = 2, \beta = 0.9$ . (e) Finally, more states become bound states where the energy level pattern becomes  $(e, o), (e, o), \dots$  in the weak QT regime. There is a shift by exact one period from (b) to (e). The maximum gap at  $\alpha = 0$  are given by Eqn.8,9 for scattering states, Eqn.15,16, Eqn.20,23 for bound states and decrease from (b) to (e). The atomic energy also increases, but becomes flat since the second bound state forms at  $l = 1$  in (d). The photon and number correlation functions from (b) to (e) are given in [38], and Eqn.26,27 respectively and could be detected by corresponding experiments. This evolution from (b) to (e) is precisely observed in the ED in Fig.6 and fine structures in all the doublets at  $l = 0, 1, 2$  shown in Fig.7,8,9. The higher energy optical modes are not shown. As explained in the caption of Fig.2, the  $U(1)$  regime may disappear if  $\beta$  [16] gets too close to 1 as in Fig.9.

different than the PPP, but similar to POC. (3) There are two minima inside the range  $0 < \theta_+ < 2\pi$  instead of just one. In this regard, it is different than the POC, but similar to the  $\phi^4$  theory. So the present quantum tunneling problem is a new class one. Furthermore, it is also very important to consider the effects of Berry phase which change the action of instanton to  $S_{int} = S_0 + i\alpha\pi$ , that of anti-instanton to  $\bar{S}_{int} = S_0 - i\alpha\pi$  (Fig.4) where  $-1/2 < \alpha < 1/2$  is the Berry phase in Eqn.4. Taking into account the differences of the present problem from the DWP, PPP and POC studied perviously in [39], es-

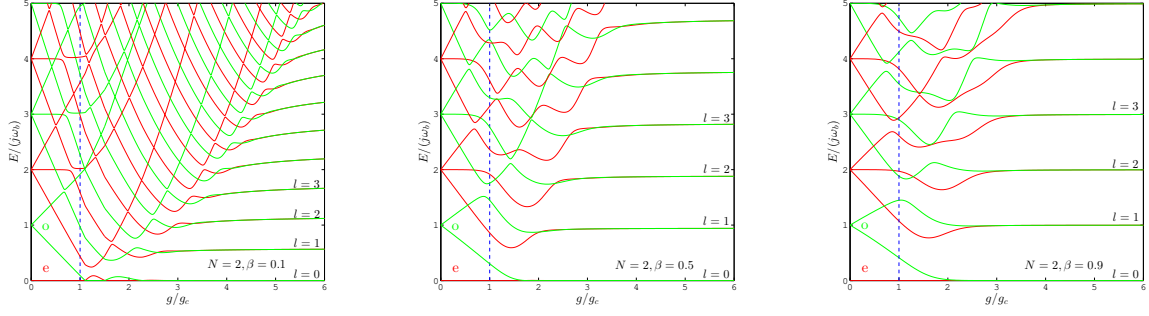


FIG. 6. ED results for the energy levels at  $N = 2, \beta = 0.1, 0.5, 0.9$  for (a),(b) and (c) respectively. (a) For  $\beta = 0.1$ , one can see there are considerable ranges of the  $U(1)$  regime  $g_c < g < g_{c1}$  before the first bound state formation at  $l = 0$  in Fig.5b, then it evolves to the strong QT where the bound states start to form at  $g_{c1}, g_{c2}, g_{c3}, \dots$  at  $l = 0, 1, 2, \dots$  in Fig.5c ( which are at the points where the energy levels at  $l = 0, 1, 2, \dots$  become approximately flat , not shown here for simplicity, but shown in the  $Z_2$  limit  $\beta = 1$  in Fig.10 ), then weak QT regime in Fig.5d as  $g/g_c$  increases. See Fig.7 for the fine structures of the doublets at  $l = 0, 1, 2$ . (b) For  $\beta = 0.5$ , the  $U(1)$  regime becomes much smaller. See Fig.8 for the fine structures of the doublets at  $l = 0, 1, 2$ . (c) For  $\beta = 0.9$ , the  $U(1)$  disappears. The bound states form after  $g_{c1}, g_{c2}, \dots$  shown in Fig.10. See Fig.9 for the fine structures of the doublets at  $l = 0, 1, 2$ . For any  $l$ , it must start with the odd parity ground state in (a)-(c). There are also none, one and two level crossing(s) in the normal regime at  $l = 0, 1, 2$  respectively. When expanding the doublets at  $l = 0, 1, \dots$ , one can see that as  $g/g_c$  increases, there are infinite energy level crossings leading to the oscillations of parities at the ground states at  $l = 0, 1, \dots$  sub-manifolds as shown in Fig.7,8,9.

pecially the crucial effects of the Berry phase, we can

evaluate the transition amplitude from  $\theta_+ = 0$  to  $\theta_+ = \pi$  in Fig.4:

$$\begin{aligned} \langle \pi | e^{-H\tau} | 0 \rangle &= \left( \frac{\omega_{-0}}{\pi D \hbar} \right)^{1/2} e^{\omega_{-0}\tau/2} \sum_{n_1, n_2} \frac{(JK e^{-S_{int}\tau})^{n_1}}{n_1!} \frac{(JK e^{-\bar{S}_{int}\tau})^{n_2}}{n_2!} \delta_{n_1 - n_2, odd} \\ &= \left( \frac{\omega_{-0}}{\pi D \hbar} \right)^{1/2} e^{\omega_{-0}\tau/2} \frac{1}{2} [e^{2JK\tau e^{-S_0} \cos \alpha \pi} - e^{-2JK\tau e^{-S_0} \cos \alpha \pi}] \end{aligned} \quad (13)$$

where  $n_1$  ( $n_2$ ) is sum over the instanton ( anti-instanton ),  $J = (S_0/2\pi\hbar)^{1/2}$  and  $K$  is the ratio of two relevant determinants to remove the zero mode of the instantons due to its center  $\tau_0$  in Eqn.4. It can be shown that  $K = C_0\omega_{-0}$  where  $C_0 = 2$  is extracted from the asymp-

totic form of the instanton solution in the  $\tau \rightarrow \infty$  limit listed above Eqn.12. Similarly, in finding the transition amplitude from 0 back to 0, one only need to change  $\delta_{n_1 - n_2, odd}$  to  $\delta_{n_1 - n_2, even}$  in the first line, then the  $-$  sign to the  $+$  sign in the second line in Eqn.13.

The two transition amplitudes lead to the Schrodinger " Cat " state with even/odd parity and the energy  $E_{e/o} = \frac{\hbar\omega_{-0}}{2} \mp \Delta_0/2$ :

$$\begin{aligned} |e\rangle_{0,SC} &= A(|\theta_+ = 0\rangle + |\theta_+ = \pi\rangle), \\ |o\rangle_{0,SC} &= A(|\theta_+ = 0\rangle - |\theta_+ = \pi\rangle), \end{aligned} \quad (14)$$

where the overlapping coefficient is  $A^2 = \frac{1}{2} \left( \frac{\omega_{-0}}{\pi \hbar D} \right)^{1/2}$ . In fact, it is important to realize that the Berry phase  $\alpha$  is defined [15, 16] at a given sector  $P$ . So Eqn.14 has a background parity  $\Pi = (-1)^P$ . So there is an oscillating parity in Eqn.14 as  $g$  increases.

The splitting between the odd and even state in Fig.3a

is:

$$\Delta_0(\alpha) = 8\omega_{-0}(\cos \alpha \pi) \left( \frac{\omega_{-0}}{\pi D} \right)^{1/2} e^{-\frac{2\omega_{-0}}{D}} \sim \sqrt{N} e^{-cN} \quad (15)$$

Similar to the  $U(1)$  regime, the Berry phase also leads to the oscillation of the gap and parity in Eqn.14. It vanishes at the two end points  $\alpha = \pm 1/2$  and reaches maximin at the middle  $\alpha = 0$ . At the first appearance of the bound state  $g_{c1}$  where  $\frac{\omega_{-0}}{D} = \frac{\pi}{4}\hbar$ , one can make a simple estimate on the upper bound value of  $\Delta_0$ :  $\Delta_0 \sim 4e^{-\pi/2}\omega_{-0} \sim 0.8\omega_{-0}$ .

Because the Berry phase effects remain in the given  $P$  sector, extending the results in Ref.[40], we find the

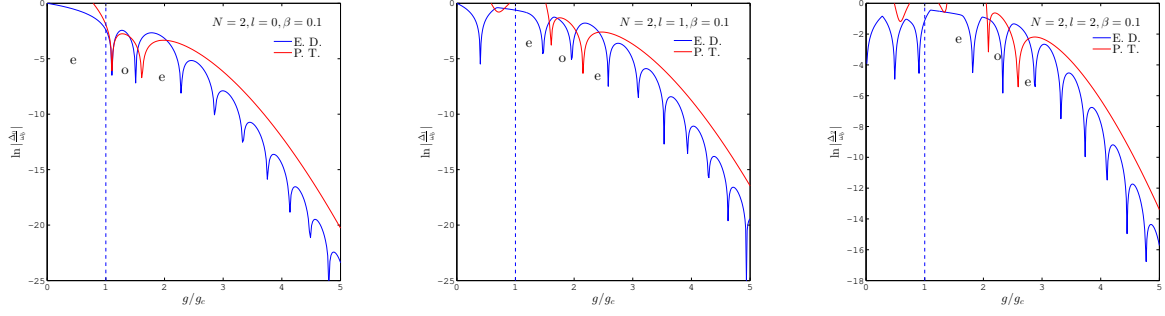


FIG. 7. In the Log scale, the even/odd splitting for  $N = 2, \beta = 0.1$  at  $l = 0, 1, 2$  calculated by strong coupling expansion ( red line ) Eqn.20 for  $l = 0$  and Eqn.23 for  $l > 0$  versus that by the ED ( blue line ). The labels  $e$  and  $o$  are the parity of the ground states. The strong coupling results do not match well with those from ED in the first  $N = 2$  zeros at  $\beta = 0.1$  in the  $U(1)$  regime. This causes no concerns because the agreement is not expected in the  $U(1)$  regime too close to  $g_c$ . Compare with Fig.6a, the first  $N = 2$  zeros at  $l = 0, 1, 2$  are certainly due to the scattering states in the  $U(1)$  regime in Fig.5b. It must start with the odd parity state at  $l = 0, 1, 2$ . The first even parity is in the normal regime in Fig.6a. Note also the changes of the scales in the vertical axis at the Log scale telling the splitting increases as  $l = 0$  to  $l = 1$ , then to  $l = 2$  as dictated by Eqn.8,9 for the scattering states. There are also none, one and two level crossing(s) in the normal regime at  $l = 0, 1, 2$  respectively. The ED gives infinite number of zeros after the first  $N = 2$  zeros which can only be achieved from higher order perturbation calculations in the strong coupling limit.

splitting in the  $n$ -th excited bound states (  $n = 0, 1$  in Fig.3b ):

$$\Delta_n(\alpha) = \frac{1}{n!} \left( \frac{8\omega_{-0}}{D} \right)^n \Delta_0 \quad (16)$$

where  $n = 0, 1, 2, \dots$  with the corresponding  $n$ -the Schrodinger "Cat" state with even/odd parity and the

energy  $E_{e/o,n} = (n + \frac{1}{2})\hbar\omega_{-0} \mp \Delta_n/2$ :

$$\begin{aligned} |e\rangle_{n,SC} &= \frac{1}{\sqrt{2}}(|n\rangle_L + |n\rangle_R), \\ |o\rangle_{n,SC} &= \frac{1}{\sqrt{2}}(|n\rangle_L - |n\rangle_R), \end{aligned} \quad (17)$$

where  $|n\rangle_{L/R}$  is the  $n$ -th bound state in the left(right) well in Fig.3a,b. Putting  $n = 0$  and projecting to the coordinate space recovers Eqn.14. One can see the higher the bound state in the Fig.3, the larger the splitting is. The main difference than the energy level pattern in the  $U(1)$  regime is that all the bound states have the  $(e, o), (e, o), \dots$  ( or  $(o, e), (o, e), \dots$  ) pattern in Fig.5d. This important observation will be substantiated further from the strong coupling expansions in the following sections.

### 5. Strong coupling expansion—

In the strong coupling limit, it is more convenient to start from the  $Z_2$  limit with  $\beta = 1$ , then treat  $1 - \beta$  as a small parameter, one can rewrite Eqn.1 as

$$\begin{aligned} H_{Z_2/U(1)} &= \omega_a a^\dagger a + \omega_b J_z + \frac{g(1+\beta)}{\sqrt{N}}(a^\dagger + a)J_x \\ &\quad - \frac{g(1-\beta)}{\sqrt{N}}(a^\dagger - a)iJ_y \end{aligned} \quad (18)$$

which can be considered as a (  $Z_2/U(1)$  ) dual presentation of the original  $U(1)/Z_2$  presentation Eqn.1. With the dual relations  $\beta \leftrightarrow 1 - \beta$  and quantum numbers  $(l, m), l = 0, 1, \dots, N; m = -P, -P + 1, \dots \leftrightarrow (m, l), m = -j, \dots, j, l = 0, 1, \dots$  where the first (second) number

stands for the optical and atomic sector in the  $U(1)/Z_2$  and  $Z_2/U(1)$  representations respectively.

After performing a rotation around the  $J_y$  axis by  $\pi/2$ , one can write  $H = H_0 + V$  where  $H_0 = \omega_a a^\dagger a + \frac{g(1+\beta)}{\sqrt{N}}(a^\dagger + a)J_z$  and the perturbation  $V = -\frac{\omega_b}{2}[J_+(1 + \lambda(a^\dagger - a)) + J_-(1 - \lambda(a^\dagger - a))]$  where  $\lambda = \frac{g(1-\beta)}{\omega_b \sqrt{N}}$  is a dimensionless parameter of order 1 when  $1 - \beta$  is small in the large  $g$  limit. The strong coupling expansion is performed in the large  $g$  limit, but with a small  $1 - \beta$  such that  $\lambda$  is of order 1.

Define  $A = a + GJ_z$  where  $G = \frac{g(1+\beta)}{\omega_a \sqrt{N}}$ , then  $H_0 = \omega_a[A^\dagger A - (GJ_z)^2]$  [12, 41]. Because  $[A, J_z] = 0$ , we denote the simultaneous eigenstates of  $A$  and  $J_z$  as

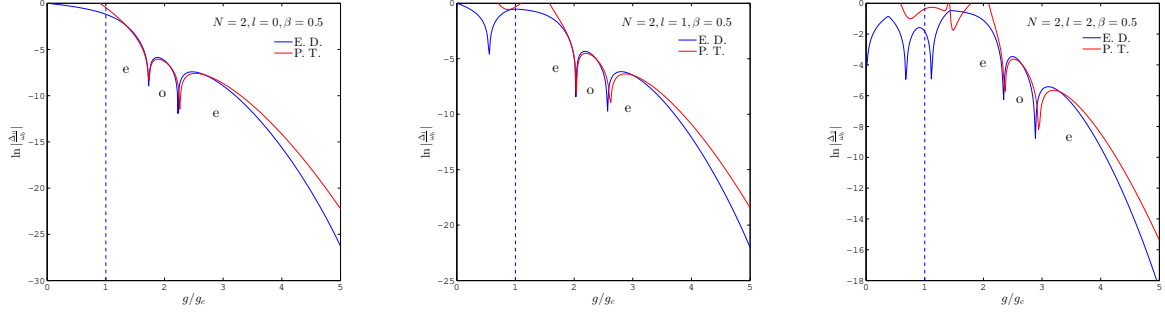


FIG. 8. In the Log scale, the even/odd splitting for  $N = 2, \beta = 0.5$  at  $l = 0, 1, 2$  calculated by strong coupling expansion ( red line ) Eqn.20 for  $l = 0$  and Eqn.23 for  $l > 0$  versus those by the ED ( blue line ). The strong coupling results match very well with those from ED in the first  $N = 2$  zeros even at  $\beta = 0.5$ . The other zeros are far apart from the first  $N = 2$  zeros and out of the scope in the figure. Compare with Fig.6b, the first  $N = 2$  zeros at  $l = 0, 1, 2$  are still due to the scattering states in the narrow  $U(1)$  regime in Fig.5c. It is a pleasant surprise that the strong coupling expansion even work very well and reproduce precisely the Berry phase effects in the  $U(1)$  regime not too close to  $g_c$ . It must start with the odd parity ground state at  $l = 0, 1, 2$ . The first even parity is in the normal regime in Fig.6b. As shown in Fig.5c, there are shifts of zeros to the right if one follow the ground state with the odd parity. Note also the changes of the scales in the vertical axis at the Log scale telling the splitting increases considerably as  $l = 0$  to  $l = 1$ , then to  $l = 2$  as dictated by Eqn.9 for the scattering states. There are also none, one and two level crossing(s) in the normal regime at  $l = 0, 1, 2$  respectively.

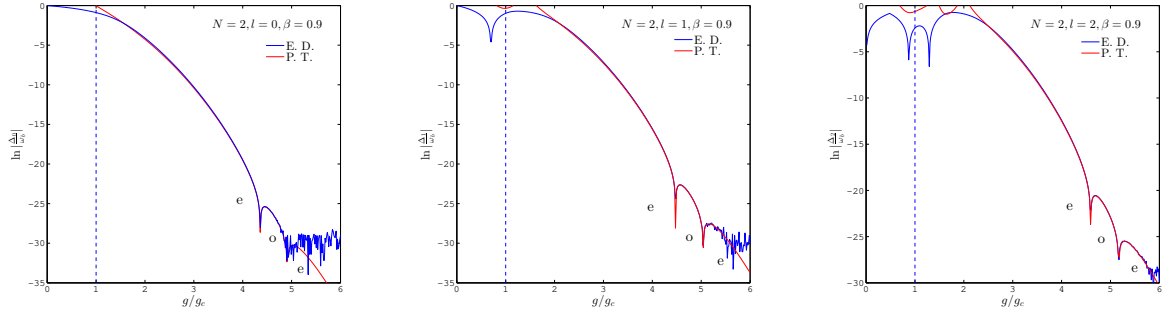


FIG. 9. In the Log scale, the even/odd splitting for  $N = 2, \beta = 0.9$  at  $l = 0, 1, 2$  calculated by strong coupling expansion ( red line ) Eqn.20 for  $l = 0$  and Eqn.23 for  $l > 0$  versus those by the ED ( blue line ). The match is essentially perfect in the first  $N = 2$  zeros at  $\beta = 0.9$  in the QT regime. The other zeros are far apart from the first  $N = 2$  zeros and out of the scope in the figure. At too strong couplings, the ED may become ( noise ) un-reliable due to the cutoff introduced in the numerical calculation. Compare with Fig.6c, all the zeros are well beyond  $g_{c1}, g_{c2}, g_{c3}, \dots$ , so the first  $N = 2$  zeros are the first two bound states at  $l = 0, 1, 2$  in the QT regime in Fig.2 and 5d. There is no  $U(1)$  regime. It must start with the odd parity ground state at  $l = 0, 1, 2$ . The first even parity is due to the bound state before the first zero in Fig.6c. Their locations are nearly independent of  $l$  as dictated by Eqn.16 or Eqn.23 for the bound states. Note also the changes of the scales in the vertical axis at the Log scale telling the splitting increases considerably as  $l = 0$  to  $l = 1$ , then to  $l = 2$  as dictated by Eqn.16 or Eqn.23 for the bound states. There are also none, one and two level crossing(s) in the normal regime at  $l = 0, 1, 2$  respectively.

$|l\rangle_m |jm\rangle, m = -j, \dots, j, l = 0, 1, \dots$ . The eigenstates satisfy  $J_z |jm\rangle = m\hbar |jm\rangle, A_m^\dagger A_m |l\rangle_m = l |l\rangle_m$  where  $A_m = a + Gm, |l\rangle_m = D^\dagger(g_m) |l\rangle = D(-g_m) |l\rangle, g_m = mG$  where  $|l\rangle$  is just the  $l$ -photon Fock state. Particularly, the ground state  $|0\rangle_m = D(-g_m) |0\rangle$  is a photon coherent state. The zeroth order eigen-energies are  $H_0 |l\rangle_m |jm\rangle = \omega_a [l - g_m^2]$ . Using the parity operator  $\Pi = e^{i\pi(a^\dagger a - J_x)}$ , one can show that  $\Pi |l\rangle_m |jm\rangle = (-1)^l |l\rangle_{-m} |j, -m\rangle$ . Because the parity is a conserved quantity at any finite  $N$ . All the eigenstates may be grouped into even or odd under

the parity operator.

$$\begin{aligned}
 |e\rangle &= \frac{1}{\sqrt{2}} [|l\rangle_m |j, m\rangle + (-1)^l |l\rangle_{-m} |j, -m\rangle] \\
 |o\rangle &= \frac{1}{\sqrt{2}} [|l\rangle_m |j, m\rangle - (-1)^l |l\rangle_{-m} |j, -m\rangle] \quad (19)
 \end{aligned}$$

The ground state is a doublet at  $|l = 0\rangle_{\pm j} |j, \pm j\rangle$ . In the large  $g$  limit, the excited states can be grouped into two sectors: (1) The atomic sector with the eigenstates  $|l > 0\rangle_{\pm j} |j, \pm j\rangle$  and energies  $l\omega_a$ . The first excited state with the energy  $\omega_a$  is the remanent of the pseudo-Goldstone mode in the  $U(1)$  regime in Fig.2a. (2) The



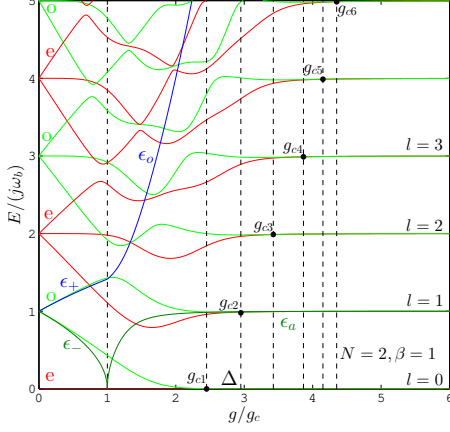


FIG. 10. The ED results for the energy levels of the  $Z_2$  Dicke model at  $N = 2$  and the  $Z_2$  limit  $\beta = 1$ . The three energy scales  $\epsilon_o, \epsilon_a, \Delta$  are shown in the figure. The labels on the vertical axis are the parity even (e) and odd (o) alternatively. There are consecutive energy level mergings estimated at  $g_c < g_{c1} < g_{c2} < \dots$  shown in Fig.3a,b. The slight energy splittings between the even and odd states are given by the quantum tunneling energy  $\Delta_l(\lambda = 0)$  in Eqn.21,23. Compared to Fig.7,8,9, there are no  $U(1)$  regime, no level crossing between the even and odd parity pairs. The ground state patterns is  $(e, o), (e, o), \dots$ . As  $\beta \rightarrow 1^-$ , all the zeros in Fig.9 are pushed to infinity. Indeed, the  $Z_2$  limit at  $\beta = 1$  has no extra symmetry than at  $0 < \beta < 1$ . At  $J = \infty$ , all the  $g'_c$ 's collapse to  $g_c, \Delta = 0$ , but the  $\epsilon_o, \epsilon_a$  stay finite [12].

optical sector with the eigenstates  $|l\rangle_m |j, m\rangle, |m| < j$  and the energies  $-\omega_a G^2 m^2$ . The first excited state with the energy  $\omega_o = \omega_a G^2 (2j - 1) = \frac{g^2(1+\beta)^2}{\omega_a} (2j-1)$  is the remnant of the Higgs mode in the  $U(1)$  regime. So in the strong coupling limit, there is wide separation between the atomic sector and the optical sector. This makes the following strong coupling expansion very effective to explore the physical phenomena in the weak QT regime in Fig.2.

#### 6. Ground state ( $l = 0$ ) splitting in the weak QT regime

The two degenerate ground state in the  $l = 0$  are  $|1\rangle = |l = 0\rangle_{-j} |j, -j\rangle, |2\rangle = |l = 0\rangle_j |j, j\rangle$  with the zeroth order energy  $E_0 = -\omega_a (Gj)^2$ . Then we can determine the matrix elements in the  $2 \times 2$  matrix which is the effective Hamiltonian projected onto the 2 dimensional subspace. One only need a second order perturbation to find a non-zero diagonal matrix element  $V_{11} = V_{22} = V_0(\lambda) = -\frac{\omega_b^2}{\omega_a} \frac{2j}{2j-1} \frac{1+\lambda^2}{G^2} < 0$ . However, one need to perform a  $N = 2j$  order perturbation to find the first non-zero contribution to the off-diagonal matrix

element  $V_{12} = V_{21} = \Delta_0(\lambda)$ :

$$\Delta_0(\lambda) = -\frac{N^2 \omega_b}{2} \left( \frac{\omega_b}{2\omega_a G^2} \right)^{N-1} e^{-(NG)^2/2} \times \sum_{l=0}^N \frac{\lambda^l}{(N-l)!} \sum_{n=0}^{[l/2]} \frac{(-1/2)^n (-NG)^{l-2n}}{n!(l-2n)!} \quad (20)$$

where  $[l/2]$  is the closest integer to  $l/2$ .

Setting  $\lambda = 0$  in Eqn.20 leads to the splitting in the  $Z_2$  Dicke model at  $\beta = 1$  ( Fig.10 ):

$$\Delta_0 = -\frac{\omega_b}{(N-1)!} \left( \frac{\omega_b}{2\omega_a} \right)^{N-1} \frac{2g^2}{\omega_a^2} e^{-N \frac{2g^2}{\omega_a^2}} < 0 \quad (21)$$

which is always a negative quantity, so leads to the even ( odd ) parity as the ground state and the first excited state respectively in Fig.10. The zero-th order ground states with even and odd parities of the system is at  $l = 0$  sector in Eqn.19:

$$|e\rangle_0 = \frac{1}{\sqrt{2}} [|l = 0\rangle_j |j, j\rangle + |l = 0\rangle_{-j} |j, -j\rangle] \\ |o\rangle_0 = \frac{1}{\sqrt{2}} [|l = 0\rangle_j |j, j\rangle - |l = 0\rangle_{-j} |j, -j\rangle] \quad (22)$$

with the energies  $E_{o/e} = E_0 + V_0 \pm |\Delta_0|$ .

Now we study the dramatic effects of the anisotropy  $\lambda > 0$  encoded in Eqn.20. If removing the exponential factor  $e^{-(G')^2/2}$ , Eqn.20 is a  $2N$ -th polynomial of  $g$ . We find that it always has  $N$  positive zeros in  $g$  beyond the  $g_{c1}$  ( namely, fall into the QT regime ). As shown in Fig.7,8,9, the positions of  $N$  zeros in Eqn.20 always match the first  $N$  zeros from ED very well. Considering higher orders perturbations, it should lead to infinite series of other zeros at larger  $g$ . This is indeed observed by the ED. However, the ED may not be precise anymore when  $g$  gets too close to the upper cut-off introduced in the ED calculation as shown in Fig.9. Any changing of sign in  $\Delta_0(\lambda)$  leads to the exchange of the parity in the ground state in Eqn.22 with energies  $E_{o/e} = E_0 + V_0(\lambda) \pm |\Delta_0(\lambda)|$ . So any  $\lambda > 0$  will lead to infinite number of level crossings with alternative parities in the ground state. This picture is consistent with the Berry phase interference effects in the instanton tunneling process discovered in the previous sections.

#### 7. Doublet splitting at $l > 0$ in the weak QT regime.

Now, we look at the energy splitting at  $l > 0$ . The diagonal matrix element at  $l = 0$  can be easily generalized to  $l > 0$  case:  $V_{11} = V_{22} = V_l(\lambda) = -\frac{\omega_b^2}{\omega_a} \frac{2j}{2j-1} \frac{1+\lambda^2(2l+1)}{G^2} < 0$ . We also find a general expression for the off-diagonal matrix element  $V_{12} = V_{21} = \Delta_l(\lambda)$ . In the  $G \gg 1$  limit, it can be simplified to:

$$\Delta_l(\lambda) \sim \frac{(-1)^l}{l!} (G'^2)^l \Delta_0(\lambda) \quad (23)$$

where  $\Delta_0(\lambda)$  is given in Eqn.20. It is enhanced due to the large prefactor  $G'^{2l}$ . Compared to Eqn.16, there is

an extra oscillating sign  $(-1)^l$  which is crucial to reconcile the results achieved from the two independent approaches! It is this oscillating sign  $(-1)^l$  which leads to the even/odd parity state at the  $l$ -th level:

$$\begin{aligned} |e, l\rangle &= \frac{1}{\sqrt{2}}[|l\rangle_j |j, j\rangle + (-1)^l |l\rangle_{-j} |j, -j\rangle] \\ |o, l\rangle &= \frac{1}{\sqrt{2}}[|l\rangle_j |j, j\rangle - (-1)^l |l\rangle_{-j} |j, -j\rangle] \end{aligned} \quad (24)$$

with the energies  $E_{o/e} = E_l^0 + V_l \pm |\Delta_l|$ ,  $E_l^0 = \omega_a[l - (Gj)^2]$ .

The important relation Eqn.23 shows that the number of zeros (remains to be  $N$ ) and the positions of the zeros are independent of  $l$ . This is indeed confirmed by the ED shown in Fig.9 for  $N = 2, \beta = 0.9, l = 0, 1, 2, 3, 4$  where the number of zeros are indeed  $N$  and the positions of zero only depend on  $l$  very weakly. So between the two

zeros, at  $l = 0, 1, 2, \dots$ , the energy levels are in the pattern  $(e, o), (e, o), \dots$  when  $\Delta_0(\lambda) < 0$  (or  $(o, e), (o, e), \dots$  when  $\Delta_0(\lambda) > 0$ ) in Fig.5d. This important result is completely consistent with the Berry phase effects in the instanton tunneling process shown in Fig.4. The fact that the same fantastic phenomena are reached from two independent analytic approaches, then confirmed by ED indicates that the results are correct, independent of the approximations we made.

#### 8. Photon, squeezing and number correlation functions in the QT regime—

In order to calculate the photon correlation functions in the strong coupling limit, one not only need to find the energy levels as done in the previous sections, but also the wavefunctions to be done in this section. Using straightforward non-degenerate perturbation expansion, we find the first order correction to the even/odd ground states at  $l = 0$  in Eqn.22:

$$\begin{aligned} |\alpha\rangle_1 &= \frac{\omega_b}{2\omega_a} \sqrt{2j} \sum_l \frac{j-1 \langle l|1 - \lambda(a^\dagger - a)|l=0\rangle_j}{l + G^2(2j-1)} \frac{1}{\sqrt{2}} [|l\rangle_{j-1} |j, j-1\rangle + \alpha(-1)^l |l\rangle_{-j+1} |j, -j+1\rangle] \\ &+ \left(\frac{\omega_b}{2\omega_a}\right)^2 2j \sum_{l, l' \neq 0} \frac{j \langle l'|1 + \lambda(a^\dagger - a)|l\rangle_{j-1} \langle l|1 - \lambda(a^\dagger - a)|l=0\rangle_j}{l'[l + G^2(2j-1)]} \frac{1}{\sqrt{2}} [|l'\rangle_j |j, j\rangle + \alpha(-1)^{l'} |l'\rangle_{-j} |j, -j\rangle] \end{aligned} \quad (25)$$

where  $\alpha = \pm$  for  $\alpha = e/o$  respectively. Indeed, it shows that the even (odd) parity ground state is mixed with only other even (odd) parity states as dictated by the parity conservation of the Hamiltonian. One can see the first-order correction to the ground state wavefunction consists of two parts: the first part (line) is in the high energy optical sector, the second part (line) is in the low energy atomic sector. Similarly, we find the first order correction to the two doublets at  $l = 1$  in Eqn.24 by (1) changing  $|l=0\rangle_j$  to  $|l=1\rangle_j$  (2) the denominator  $[l + G^2(2j-1)]$  to  $[l-1 + G^2(2j-1)]$ . (3) the sum subscript  $l' \neq 0$  to  $l' \neq 1$ .

Using the Lehmann representations, we find there is no first order correction to the photon normal correlation function, but there is one to the anomalous photon correlation function:

$$\begin{aligned} \langle a(\tau)a^\dagger(0) \rangle &= Ae^{-\Delta_0\tau} + e^{-(\omega_a + \Delta_a)\tau} \\ \langle a(\tau)a(0) \rangle &= Ae^{-\Delta_0\tau} - Be^{-(\omega_a + \Delta_a)\tau} \end{aligned} \quad (26)$$

where  $A = (Gj)^2 = N \frac{g^2(1+\beta)^2}{4\omega_a^2}$ ,  $B = \frac{\lambda^2}{G^2} \left(\frac{\omega_b}{2\omega_a}\right)^2 \frac{2j}{2j-1}$  and  $\Delta_a = (V_1 - V_0) + \frac{1}{2}(\Delta_1 + \Delta_0)$ . One can see the anomalous spectral weight in the atomic mode is completely due to  $\lambda$ , which can be easily detected in phase sensitive Homodyne measurements [36].

Similarly, we also find the first order correction to the photon number correlation function:

$$\langle n(\tau)n(0) \rangle - \langle n \rangle^2 = A[1 + B]^2 e^{-(\omega_a + \Delta_n)\tau} \quad (27)$$

where  $\Delta_n = (V_1 - V_0) - \frac{1}{2}(\Delta_1 - \Delta_0)$  and  $\langle n \rangle = A$  is the photon number in the ground state and does not receive first-order correction.

Second order corrections to the photon normal and anomalous correlation functions in Eqn.26 and photon number correlation function in Eqn.27, the first and second order to the optical spectral weights due to the first line in Eqn.25 will be computed in [38].

#### 9. Experimental implications—

As shown in [16], in real experiments of superconducting qubits or quantum dots inside a cavity in Fig.1b, there are always the potential scattering term  $\lambda_z J_z a^\dagger a / j$  between the cavity photons and the qubits and the qubit-qubit interaction term  $u J_z^2 / j$ . The critical coupling  $g_c$  at  $N = \infty$  is reduced to:

$$g_c = \sqrt{(\omega_a - \lambda_z)(\omega_b - 2u)} / (1 + \beta) \quad (28)$$

which indicates that the two repulsive interaction terms can be used to decrease the critical  $g_c$  well below the bare critical strength  $\sqrt{\omega_a \omega_b} / (1 + \beta)$ . The qubit-qubit interactions can be tuned inductively or capacitively. This fact could be used to put the system into at least the strong QT regime in Fig.2 in the near future experiments using both atoms inside a optical cavity in Fig.1a or qubits inside a microwave circuit QED in Fig.1b.

(a) Coherent switching between the even and odd parity state in Fig.3.

With  $N \sim 10^5$  atoms of  $^{87}\text{Rb}$  inside a cavity [27–29], the system is in the thermodynamic limit, so the novel physical phenomena in the  $U(1)$  and QT regime in Fig.2 at finite small  $N$  explored in this work are hard to observe. However, with the recent advances of manipulating a few atoms [32, 33], the number of atoms can be reduced to a few to a few hundreds, then the  $U(1)$  and the QT regime in Fig.2, Fig.3a,b span a large parameter regimes. We expect the rich physics in both regimes can be probed in future experiments. The Goldstone and Higgs modes in the  $U(1)$  regime was discussed in [16] and drawn in Fig.5b. Here, we focus on the QT regime. For example, the experiment [29] ( for  $Z_2$  Dicke model at  $\beta = 1$  ) first adiabatically prepared the system in one of the two bound states in Fig.3b by applying a small  $Z_2$  symmetry breaking field, then **turn off and on** the transverse pumping laser in Fig.1a and observed the coherent switch with the frequency  $\omega_b$  between the two ground states in Fig.3b by an optical heterodyne detection. In a future experiment with only a few to a few hundreds atoms[32, 33], one can first adiabatically prepare the system in one of the two bound states in Fig.3b, but still **keep** the transverse pumping laser in Fig.1a, then observe by the optical heterodyne detection the coherent oscillation probability between the two bound states  $P(t) = \cos \Delta_0 t$  where the  $\Delta_0$  is given by Eqn.15 at  $\alpha = 0$ .

(b) The continuously tunable Schrodinger Cats

There have been extensive efforts to realize the Schrodinger Cat state in trapped ions [43] and superconducting qubit systems [44]. Here, we showed that the Schrodinger Cats in Eqn.14 or 17 prepared in the strong QT regime in Fig.2a can be continuously tuned from  $N \sim 3 - 9$  as shown in Fig.3a,b, it involves all the  $N$  number of atoms ( qubits ) and photons strongly coupled inside the cavity and could have important applications in quantum information processions.

(c) Observing the Berry phase effects of the instanton tunneling events at  $0 < \beta < 1$ .

As emphasized in this work, in order to observe the Berry phase interference effects, one has to move away from the  $Z_2$  limit realized in the experiments [27–29], namely,  $0 < \beta < 1$ . This has been at least attempted in the recent experiment [31] which can tune  $g$  and  $g'$  independently. If the number of atoms can be reduced to a few [32, 33], then the dramatic Berry phase effects in the oscillating frequency between the even/odd party ground state  $P(\alpha, t) = \cos \Delta_0(\alpha)t$  can be observed. As shown in Eqn.15, the Berry phase  $-1/2 < \alpha < 1/2$  can be continuously tuned by the atom-photon interaction.

The advantage of the superconducting qubits in Fig.1b over the cold atoms in Fig.1a is that the two level ( qubit ) or three level ( qutrit ) approximation is much more robust than the former. In circuit QED systems, there are also various experimental set-ups such as charge, flux, phase qubits or qutrits, the couplings could be capacitive or inductive through  $\Lambda, V, \Xi$  or the  $\Delta$  shape [42].

Especially, continuously changing  $0 < \beta < 1$  has been achieved in the recent experiment [26]. Then all the interesting phenomena in the  $U(1)$  and QT regime in Fig.2 at a finite  $N = 3 - 9$  qubits, especially the Berry phase effects can be observed in near future experiments.

(d) Detections of leaking photon characteristics.

All the parameters of the cavity systems such as the doublet splittings  $\Delta_0(\lambda), \Delta_1(\lambda)$  and energy shifts  $V_1 - V_0$  are encoded in the photon normal and anomalous Green functions Eqn.26 and photon number correlation functions Eqn.27 which can be measured by photoluminescence, phase sensitive homodyne and Hanbury-Brown-Twiss ( HBT ) type of experiments [36]. From Eqn.26 and 27, one can see  $\Delta_a + \Delta_n = 2(V_1 - V_0) + \Delta_0, \Delta_a - \Delta_n = \Delta_1$ . So  $\Delta_0(\lambda), \Delta_1(\lambda)$  and the energy shifts  $V_1 - V_0$  can all be measured.

10. Conclusions—

Quantum optics differs from condensed matter physics at least in two important ways (1) the former mainly deal with finite sized systems, while the latter mainly deal with thermodynamic limit ( or edge states if there is a bulk topological order ) (2) the former mainly study pumping-decay non-equilibrium systems, while the latter mainly equilibrium systems. In this paper, we focused on the first feature. The combination of both features will be presented elsewhere. In studying the latter, one stress " More is different " as advocated by P. W. Anderson. Here, to study the four most important quantum optics models in the former system, we take the " Few is different " point of view [15, 16] which establish the connections between the many body physics in condensed matter systems and few body problems in quantum optical systems. The importance of these models in quantum optics at a finite  $N$  ranks the same as the bosonic ( fermionic ) Hubbard models and Heisenberg models in strongly correlated electron systems and the Ising models in Statistical mechanics. We introduce the most general  $U(1)/Z_2$  Dicke model which incorporates all the 4 quantum optics models as the special limits and investigate the fantastic phenomena encoded in this model at a finite  $N$  from a unified approach.

We can see some illuminating duality in the quantum numbers characterizing the excitations of the  $U(1)/Z_2$  Dicke model: In the  $U(1)$  crossover regime, the Landau level index  $l = 0, 1, \dots, N$  (  $N + 1$  Landau levels ) denotes the high energy Higgs type of excitation, the magnetic number  $m = -P, -P + 1, \dots$  ( no upper bounds ) denotes the low energy pseudo-Goldstone mode. However, in the strong coupling ( super-radiant ) regime, the Landau level index  $l = 0, 1, \dots$  ( no upper bounds ) denotes the low energy atomic excitation, the magnetic number  $m = -j, -j + 1, \dots, j$  (  $2j + 1 = N + 1$  ) denotes the high energy optical mode. So the Landau level index and the magnetic number exchanges their roles under  $\beta \leftrightarrow 1 - \beta$ .

At the  $U(1)$  limit  $\beta = 0$ , there are infinite level crossings due to the Berry phase effects at a finite  $N$  ( Fig.5a )

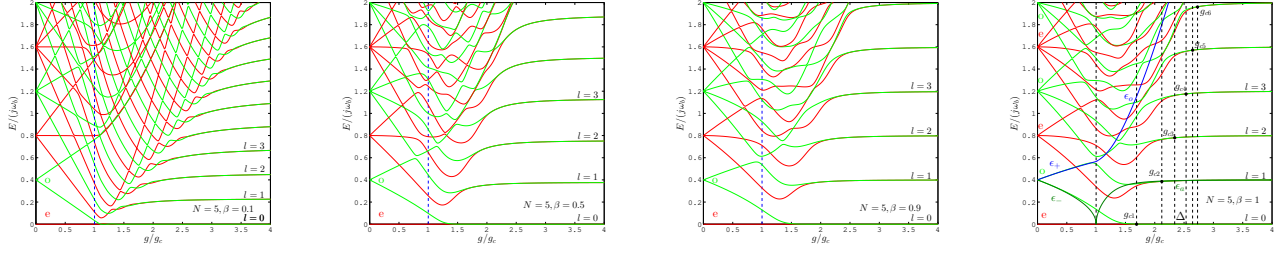


FIG. 11. ED results for the energy levels at  $N = 5, \beta = 0.1, 0.5, 0.9$  and the  $Z_2$  limit  $\beta = 1$ . One can see that the  $U(1)$  regime in Fig.5a at  $g_c < g < g_{c1}$  gradually evolves to the strong QT, then weak QT regime in Fig.5e as  $g/g_c$  increases. When expanding the two emerging levels, one can see that as  $g/g_c$  increases, there are infinite energy level crossings leading to the oscillations of parities in the ground state  $l = 0$  and also  $l > 0$  sectors. However, the oscillations disappear at the  $Z_2$  limit  $\beta = 1$ .

as first discovered in [15]. Turning on a small  $\beta$  will only lead to level repulsion between the same parity states, the Berry phase still leads to the level crossings between the even and odd state, therefore the alternating parities on the ground state and also all the levels at  $|m| = 1, \dots, P$  in the  $U(1)$  regime ( Fig.5b ). When  $\beta$  gets bigger, the system evolves into the weak quantum tunneling regime where the Berry phase continue to play a crucial role leading to interference between different tunneling events ( Fig.5c and d ). As  $\beta$  gets close to 1, the  $U(1)$  regimes disappears, the normal state directly gets to the QT regime, the Berry phase effects show up after the formations of all the bound states. At the  $Z_2$  limit  $\beta = 1, \lambda = 0$ , the Berry phase effects are pushed into infinity, so there is no level crossing in Fig.10, the energy levels satisfy Wigner-Dyson distributions in the superradiant regime [12]. However, at any  $\beta < 1$  in Eqn.18, it is the extra term  $\lambda(a^\dagger - a)iJ_y$  which introduces frustrations, therefore Berry phase effects into the  $Z_2$  Dicke model. They leads to infinite level crossings with alternating even and odd parity in the ground state and all the doublets at  $l > 1$  ( Fig.5d ). Combining the physical picture from  $\beta$  small achieved from  $U(1)$  limit by instanton method to large  $\beta \sim 1$  achieved from  $Z_2$  limit by the strong coupling expansion method [35], we conclude that it is the Berry phase effects which lead to the level crossings at any  $0 \leq \beta < 1$  except at the  $Z_2$  limit  $\beta = 1$ . Similar methods have also been applied to study corresponding  $U(1)/Z_2$  Lipkin-Meshkov-Glick (LMG) model [14, 45, 46] at a finite  $N$  inside the superradiant regime. It was shown in Ref.[47] that it is Berry phase effects in the instanton tunneling events in the 2+1 compact QED which leads to the Valence bond order in 2d quantum Anti-ferromagnet. Here we showed that it is Berry phase effects in the 0+1 dimensional instanton tunneling events in the compact phase of photons which leads to the infinite level cross-

ing with alternating parity in the ground and low energy excited states ( Fig.5,6 ).

So far, any ED needs to introduce a upper cutoff ( see Fig.9 ) to truncate the Hilbert space. If extending the solution to the Rabi model [18] at  $N = 1, \beta = 1$  to any  $N$  and  $0 < \beta < 1$  is possible, then the formally exact formal solutions maybe used to get rid of the cutoff in the ED. How to make use of these formally exact  $G$  functions to recover the novel phenomena in the  $U(1)$  and QT regimes achieved in this paper remain an outstanding problem. It is also important to study how the energy level statistics changes with  $\beta$  within a given parity in Fig.5. Most importantly, the pumping-decay effects on Fig.2 will be presented in future publications.

**Acknowledgements:** J. Ye thank Yu Chen for his participation and Prof. Guangshan Tian for encouragements in the very early stage of the project. We thank Han Pu and Lin Tian for helpful discussions. Y.Y and JY are supported by NSF-DMR-1161497, NSFC-11174210. W.M. Liu is supported by NSFC under Grants No. 10934010 and No. 60978019, the NKBRSCF under Grants No. 2012CB821300. CLZ's work has been supported by National Keystone Basic Research Program (973 Program) under Grant No. 2007CB310408, No. 2006CB302901 and by the Funding Project for Academic Human Resources Development in Institutions of Higher Learning Under the Jurisdiction of Beijing Municipality.

### Appendix

In the main text, we focused on  $N = 2, \beta = 0.1, 0.5, 0.9$ . Here we list the energy levels at  $N = 5, \beta = 0.1, 0.5, 0.9$  in Fig.11. We also made the comparisons between strong coupling expansions and the ED on the doublet splittings at  $l = 0, 1, 2$  and found similar agreements as shown in Fig.8 and 9 in the QT and  $U(1)$  regimes far away from  $g_c$ , but as expected, some discrepancies in Fig.7 in the  $U(1)$  regime close to  $g_c$ .

[2] M. O. Scully and M. S. Zubairy, Quantum Optics, Cam-

[1] D. F. Walls and G. J. Milburn, Quantum Optics, Springer-Verlag, 1994.

- bridge University press, 1997
- [3] Y. Yamamoto and A. Imamoglu, Mesoscopic quantum optics, John Wiley & Sons, Inc. 1999.
- [4] I.I. Rabi, Phys. Rev. 49, 324 (1936); 51, 652 (1937).
- [5] R.H. Dicke, Phys. Rev. 93, 99 (1954)
- [6] E. T. Jaynes and F. W. Cummings, Proc. IEEE 51, 89 (1963).
- [7] M. Tavis and F.W. Cummings, 170, 379 (1968).
- [8] K. Hepp and E. H. Lieb, Anns. Phys. ( N. Y. ), 76, 360 (1973); Y. K. Wang and F. T. Hioe, Phys. Rev. A, 7, 831 (1973).
- [9] V. N. Popov and S. A. Fedotov, Soviet Physics JETP, 67, 535 (1988); V. N. Popov and V. S. Yarunin, Collective Effects in Quantum Statistics of Radiation and Matter (Kluwer Academic, Dordrecht,1988).
- [10] P. R. Eastham and P. B. Littlewood, Phys. Rev. B 64, 235101 (2001).
- [11] V. Buzek, M. Orszag and M. Roko, Phys. Rev. Lett. 94, 163601 (2005).
- [12] C. Emary and T. Brandes, Phys. Rev. Lett. 90, 044101 (2003); Phys. Rev. E 67, 066203 (2003). N. Lambert, C. Emary, and T. Brandes, Phys. Rev. Lett. 92, 073602 (2004).
- [13] J. Vidal and S. Dusuel, Finite-size scaling exponents in the Dicke model, Europhys. Lett. 74, 817 (2006).
- [14] R. Botet, R. Jullien, and P. Pfeuty, Size Scaling for Infinitely Coordinated Systems, Phys. Rev. Lett. 49, 478 (1982); Large-size critical behavior of infinitely coordinated systems, Phys. Rec. B, 28, 3955 (1983).
- [15] Jinwu Ye and CunLin Zhang, Super-radiance, Photon condensation and its phase diffusion, Phys. Rev. A 84, 023840 (2011).
- [16] Yu Yi-Xiang, Jinwu Ye and W.M. Liu, Scientific Reports 3, 3476 (2013).
- [17] The  $U(1)$  Dicke ( Tavis-Cummings ) model is integrable at any finite  $N$ , so, in the " face " value, the system's eigen-energy spectra could be "exactly" solvable by Bethe Ansatz like methods. For example, see N.M. Bogoliubov, R.K. Bullough, and J. Timonen, Exact solution of generalized Tavis-Cummings models in quantum optics, J. Phys. A: Math. Gen. 29 6305 (1996). However, so far, the Bethe Ansatz like solutions stay at very "formal" level from which it is not known how to get the system's eigen-energy levels achieved in [15, 16] by  $1/N$  and  $1/J$  expansions, let alone to extract any underlying physics explored in these two papers. Furthermore, it is known that the Bethe Ansatz method is not able to get any dynamic correlation functions computed in the two papers.
- [18] D. Braak, Phys. Rev. Lett. 107, 100401 C Published 29 August 2011. Similar comments in [17] applied here also. It is still unknown how to extract any interesting phenomena achieved in the present paper from the formally exact solution written down in this reference even when setting  $N = 1, \beta = 1$ .
- [19] J. Ye and S. Sachdev, Phys. Rev. B 44, 10173 (1991); J. Ye, S. Sachdev and N. Read, Phys. Rev. Lett. 70, 4011 (1993); A. Chubukov, S. Sachdev and J. Ye ; Phys. Rev. B 49, 11919 (1994); Jinwu Ye and S. Sachdev; Phys. Rev. Lett. 80, 5409 (1998); Jinwu Ye, Phys. Rev. B60, 8290 (1999).
- [20] Ferdinand Brennecke, Tobias Donner, Stephan Ritter, Thomas Bourdel, Michael Khl, Tilman Esslinger, Cavity QED with a Bose-Einstein condensate , Nature 450, 268 - 271 (08 Nov 2007).
- [21] Yves Colombe, Tilo Steinmetz, Guilhem Dubois, Felix Linke, David Hunger, Jakob Reichel, Strong atom-field coupling for Bose-Einstein condensates in an optical cavity on a chip , Nature 450, 272 - 276 (08 Nov 2007).
- [22] A. Wallraff, *et.al*, Strong coupling of a single photon to superconducting qubit using circuit quantum electrodynamics, Nature 431, 162-167 (2004)
- [23] G. Gunter, A. A. Anappara, J. Hees, A. Sell, G. Biasiol, L. Sorba, S. De Liberato, C. Ciuti, A. Tredicucci, A. Leitenstorfer, R. Huber, Sub-cycle switch-on of ultrastrong light-matter interaction, NATURE, Vol 458, 178, 12 March 2009.
- [24] Aji A. Anappara1, Simone De Liberato, Alessandro Tredicucci1, Cristiano Ciuti, Giorgio Biasiol, Lucia Sorba, and Fabio Beltram, Signatures of the ultrastrong light-matter coupling regime, Phys. Rev. B 79, 201303(R) (2009).
- [25] Reithmaier, J. P, *et.al*, Strong coupling in a single quantum dot-semiconductor micro-cavity system, Nature 432, 197-200 (2004). Yoshie, T. *et al*, Vacuum Rabi splitting with a single quantum dot in a photonic crystal nanocavity, Nature 432, 200-203 (2004). K. Hennessy, A. Badolato, M. Winger, D. Gerace, M. Atatre, *et al*, Quantum nature of a strongly coupled single quantum dotC-cavity system, Nature 445, 896-899 (22 February 2007).
- [26] T. Niemczyk, *et.al*, Circuit quantum electrodynamics in the ultrastrong-coupling regime, Nature Physics 6,772C776(2010).
- [27] A. T. Black, H. W. Chan and V. Vuletic, Observation of Collective Friction Forces due to Spatial Self-Organization of Atoms: From Rayleigh to Bragg Scattering, Phys. Rev. Lett. 91, 203001(2003).
- [28] K. Baumann, *et.al*, Dicke quantum phase transition with a superfluid gas in an optical cavity, Nature 464, 1301-1306 (2010);
- [29] K. Baumann, R. Mottl, F. Brennecke, and T. Esslinger, Exploring Symmetry Breaking at the Dicke Quantum Phase Transition, Phys. Rev. Lett. 107, 140402 (2011).
- [30] F. Dimer, B. Estienne, A. S. Parkins, and H. J. Carmichael, Phys. Rev. A, 75, 013804, 2007
- [31] Markus P. Baden, Kyle J. Arnold, Arne L. Grimsmo, Scott Parkins, and Murray D. Barrett, Realization of the Dicke Model Using Cavity-Assisted Raman Transitions, Phys. Rev. Lett. 113, 020408 C Published 10 July 2014.
- [32] W. S. Bakr, *et.al*, Probing the SuperfluidCtoCMott Insulator Transition at the Single-Atom Level, Science 30 July 2010: 547-550.
- [33] F. Serwane, *et.al*, Deterministic Preparation of a Tunable Few-Fermion System, Science 15 April 2011: 336-338.
- [34] At the QCP of the  $Z_2$  Dicke model at  $\beta = 1$ , it was found in [13] that  $\langle n_{ph} \rangle \sim N^{1/3}$ . Because the normal to the superradiant transitions at  $N = \infty$  share the same universality class at all  $0 < \beta < 1$ , from finite size scaling with infinite coordination numbers [14], we expect that only the coefficient in  $\langle n_{ph} \rangle \sim N^{1/3}$  depends on  $\beta$ . As shown in this paper, the dramatic differences due to  $0 < \beta < 1$  show up only away from the QCP in all the three regimes in Fig.2.
- [35] For strong coupling expansions and spin wave expansion in spin-orbit coupled lattice systems, see Fadi Sun, Jinwu Ye, Wu-Ming Liu, arXiv:1408.3399, arXiv:1502.05338.
- [36] Jinwu Ye, T. Shi and Longhua Jiang, Phys. Rev. Lett.

- 103, 177401 (2009); T. Shi, Longhua Jiang and Jinwu Ye, Phys. Rev. B 81, 235402 (2010); Jinwu Ye, Fadi Sun, Yi-Xiang Yu and Wuming Liu, Ann. Phys. 329, 51C72 (2013).
- [37] Intuitively, one may define the Schrodinger Cats with even parity as male cats, odd parity as female cats or vice versa.
- [38] Yu Yi-Xiang, Jinwu Ye, W.M. Liu and CunLin Zhang, unpublished.
- [39] S. Coleman, Aspects of Symmetry, Cambridge University Press, 1985, A. M. Polyakov, Gauge Fields and Strings, Harwood Academic Publishers, 1987; R. Rajaraman, Solitons and Instantons, North-Holland Publishing Company, 1982
- [40] U. Weiss and W. Haffner, Phys. Rev. D 27, 2916 (1983).
- [41] Qing-Hu Chen, Yu-Yu Zhang, Tao Liu and Ke-Lin Wang, Numerically exact solution to the finite-size Dicke model, Phys. Rev. A 78, 051801(R) (2008).
- [42] For reviews, see J. Q. You, Franco Nori, Atomic physics and quantum optics using superconducting circuits, Nature 474, 589 (2011) . Steven M. Girvin, Superconducting Qubits and Circuits: Artificial Atoms Coupled to Microwave Photons, Lectures delivered at Ecole d'Ete Les Houches, July 2011 To be published by Oxford University Press.
- [43] C. Monroe, D. M. Meekhof, B. E. King, and D. J. Wineland, A Schrodinger Cat Superposition State of an Atom, Science 24 May 1996: 1131-1136; D. Leibfried, E. Knill, S. Seidelin, J. Britton, R. B. Blakestad, J. Chiaverini, D. B. Hume, W. M. Itano, J. D. Jost, C. Langer, et al, 1.Creation of a six-atom Schrödinger cat state, Nature 438, 639-642 (1 December 2005).
- [44] Jonathan R. Friedman, Vijay Patel, W. Chen, S. K. Tolpygo, J. E. Lukens, 1.Quantum superposition of distinct macroscopic states, Nature 406, 43-46 (6 July 2000). Caspar H. van der Wal, A. C. J. ter Haar, F. K. Wilhelm, R. N. Schouten, C. J. P. M. Harmans, T. P. Orlando, Seth Lloyd, and J. E. Mooij, Quantum Superposition of Macroscopic Persistent-Current States, Science 27 October 2000: 773-777.
- [45] S. Morrison and A. S. Parkins, Dynamical Quantum Phase Transitions in the Dissipative Lipkin-Meshkov-Glick Model with Proposed Realization in Optical Cavity QED, Phys. Rev. Lett. 100, 040403 C Published 31 January 2008; Collective spin systems in dispersive optical cavity QED: Quantum phase transitions and entanglement, Phys. Rev. A 77, 043810 C Published 8 April 2008.
- [46] Sbastien Dusuel and Julien Vidal, Finite-Size Scaling Exponents of the Lipkin-Meshkov-Glick Model, Phys. Rev. Lett. 93, 237204.
- [47] N. Read and S. Sachdev, Nucl. Phys. B 316, 609 (1989); Phys. Rev. Lett. 62, 1694 (1989); Phys. Rev. B 42, 4568 (1990), Phys. Rev. Lett. 66, 1773 (1991). G. Murthy and S. Sachdev, Nucl. Phys. B 344, 557 (1990).